NeuroImage: Clinical 25 (2020) 102152

Contents lists available at ScienceDirect

NeuroImage: Clinical

journal homepage: www.elsevier.com/locate/ynicl

Brain volume and flortaucipir analysis of progressive supranuclear palsy clinical variants

Jennifer L. Whitwell[a,*], Nirubol Tosakulwong[b], Hugo Botha[c], Farwa Ali[c], Heather M. Clark[c], Joseph R. Duffy[c], Rene L. Utianski[c], Chase A. Stevens[c], Stephen D. Weigand[b], Christopher G. Schwarz[a], Matthew L. Senjem[a,d], Clifford R. Jack[a], Val J. Lowe[a], J. Eric Ahlskog[c], Dennis W. Dickson[e], Keith A. Josephs[c]

[a] Department of Radiology, Mayo Clinic, Rochester, MN, United States
[b] Department of Health Sciences Research, Mayo Clinic, Rochester, MN, United States
[c] Department of Neurology, Mayo Clinic, Rochester, MN, United States
[d] Department of Information Technology, Mayo Clinic, Rochester, MN, United States
[e] Department of Neuroscience, Mayo Clinic, Jacksonville, FL, United States

ARTICLE INFO

Keywords:
MRI
Flortaucipir
PET
PSP
Atypical

ABSTRACT

Background and purpose: Progressive supranuclear palsy (PSP) is a neurodegenerative tauopathy that is associated with different clinical variants, including PSP-Richardson's syndrome (PSP-RS), PSP-parkinsonism (PSP-P), PSP-corticobasal syndrome (PSP-CBS), PSP-frontal (PSP-F), PSP-progressive gait freezing (PSP-PGF) and PSP-speech/language (PSP-SL). While PSP-RS has been well-characterized on neuroimaging, the characteristics of the other atypical variants are less well defined and it is unknown how they compare to each other or relate to neuropathology. We aimed to assess and compare regional atrophy on MRI and [^{18}F]flortaucipir uptake on PET across PSP variants.

Materials and methods: 105 PSP patients (53 PSP-RS, 23 PSP-SL, 12 PSP-P, 8 PSP-CBS, 5 PSP-F and 4 PSP-PGF) underwent volumetric MRI, with 59 of these also undergoing flortaucipir PET. Voxel-level and region-level analyses were performed comparing PSP variants to 30 controls and to each other. Semi-quantitative tau burden measurements were also performed in 21 patients with autopsy-confirmed PSP.

Results: All variants showed evidence for atrophy or increased flortaucipir uptake in striatum, globus pallidus and thalamus. Superior cerebellar peduncle volume loss was only observed in PSP-RS, PSP-CBS and PSP-F. Volume loss in the frontal lobes was observed in PSP-SL, PSP-CBS and PSP-F, with these variants also showing highest cortical tau burden at autopsy. The PSP-P and PSP-PGF variants showed more restricted patterns of neurodegeneration predominantly involving striatum, globus pallidus, subthalamic nucleus and thalamus. The PSP-SL variant showed greater volume loss and flortaucipir uptake in supplementary motor area and motor cortex compared to all other variants, but showed less involvement of subthalamic nucleus and midbrain. Compared to PSP-RS, PSP-P had larger midbrain volume and greater flortaucipir uptake in putamen.

Conclusion: The PSP variants have different patterns of involvement of subcortical circuitry, perhaps suggesting different patterns of disease spread through the brain. These findings will be important in the development of appropriate neuroimaging biomarkers for the different PSP variants.

1. Introduction

Progressive supranuclear palsy (PSP) is a neurodegenerative disorder characterized by the deposition of tau immunoreactive globose neurofibrillary tangles, coiled bodies, tufted astrocytes and threads in the brain (Dickson, 2008; Steele et al., 1964). It has been recognized for

Abbreviations: FWE, family wise error; MCALT, Mayo Clinic Adult Lifespan Template; MDS-PSP, Movement Disorders Society clinical criteria for PSP; MPRAGE, magnetization prepared rapid gradient echo; PSP, progressive supranuclear palsy; PSP-CBS, corticobasal variant of PSP; PSP-F, frontal variant of PSP; PSP-PGF, progressive gait freezing variant of PSP; PSP-RS, Richardson's syndrome; PSP-SL, speech/language variant of PSP; ROI, region of interest; SUVR, standardized uptake value ratio

* Corresponding author.
E-mail address: whitwell.jennifer@mayo.edu (J.L. Whitwell).

https://doi.org/10.1016/j.nicl.2019.102152
Received 5 October 2019; Received in revised form 25 November 2019; Accepted 26 December 2019
Available online 28 December 2019

many years that PSP can present with a number of different clinical presentations and the recently published Movement Disorders Society clinical criteria for PSP (MDS-PSP) provides guidelines for diagnosing different PSP variants (Hoglinger et al., 2017). The most common clinical presentation is PSP-Richardson's syndrome (PSP-RS) which is diagnosed by the presence of both falls early in the disease course and either slowing of vertical saccades or vertical supranuclear gaze palsy (Steele et al., 1964; Hoglinger et al., 2017; Litvan et al., 1996). However, patients with PSP can also present with other predominant clinical features, such as progressive gait freezing (PSP-PGF) (Williams et al., 2007), a Parkinson's disease phenotype (PSP-P) (Williams et al., 2005), corticobasal syndrome (PSP-CBS) (Josephs et al., 2012; Tsuboi et al., 2005), behavioral variant of frontotemporal dementia (PSP-frontal or PSP-F) (Hassan et al., 2012) or speech and language impairment (PSP-SL) (Josephs et al., 2005; 2006).

Magnetic resonance imaging (MRI) research has largely focused on studying the classic PSP-RS phenotype, showing characteristic patterns of atrophy of midbrain, subcortical grey matter structures (including striatum, thalamus and globus pallidus), and frontal lobes (Josephs et al., 2008, 2006, 2013; Boxer et al., 2006; Brenneis et al., 2004; Groschel et al., 2006; Oba et al., 2005; Paviour et al., 2005; Agosta et al., 2010; Price et al., 2004), as well as degeneration of the superior cerebellar peduncle and structures along the dentatorubrothalamic pathway (Whitwell et al., 2011, 2017, 2011, 2014; Knake et al., 2010; Padovani et al., 2006). These neuroimaging findings have concurred with pathological findings in PSP-RS (Dickson, 1999; Dickson et al., 2010). Specifically, the nuclei that are most affected pathologically in PSP-RS are the globus pallidus, subthalamic nucleus and substantia nigra, with atrophy in the midbrain and superior cerebellar peduncle; also consistently found is mild neuronal loss and gliosis in the striatum and thalamus, neuronal loss and grumose degeneration of the dentate nucleus of the cerebellum and mild atrophy of the frontal lobe (Dickson et al., 2010). Recent neuroimaging studies using PET ligands that bind to tau proteins in the brain, such as [^{18}F]flortaucipir (previously known as [^{18}F]AV-1451 (Chien et al., 2013; Xia et al., 2013)), have also shown increased uptake in the globus pallidus, midbrain, thalamus, subthalamic nucleus, and dentate nucleus of the cerebellum in PSP-RS (Cho et al., 2017; Passamonti et al., 2017; Schonhaut et al., 2017; Whitwell et al., 2018, 2017; Smith et al., 2017). Again, this matches the distribution of tau pathology observed at autopsy.

Pathological studies have shown that PSP clinical-variant subtypes are associated with different distributions of pathology across this system of structures compared to PSP-RS, with some PSP variants showing a predominance of cortical involvement and others showing greater tau pathology in the globus pallidus, diencephalon and brainstem, i.e. “brainstem predominant” (Williams et al., 2007, 2005; Josephs et al., 2005; Dickson et al., 2010; Williams et al., 2007). Less is known about the neuroimaging features of these atypical PSP variants. Midbrain atrophy has been observed in some patients with the atypical PSP syndromes (Hassan et al., 2012; Agosta et al., 2010; Longoni et al., 2011; Quattrone et al., 2016; Santos-Santos et al., 2016; Josephs et al., 2012; Whitwell et al., 2012; Rohrer et al., 2010), but not in others (Whitwell et al., 2013), and it is unclear whether the degree of atrophy differs from PSP-RS (Agosta et al., 2010; Longoni et al., 2011; Whitwell et al., 2012). Atrophy in the frontal lobes has also been observed across different syndromes, particularly PSP-SL (Josephs et al., 2006; Santos-Santos et al., 2016; Rohrer et al., 2010), PSP-F (Hassan et al., 2012) and PSP-CBS (Lee et al., 2011; Whitwell et al., 2010). However, these studies have only reported small numbers of patients, have not compared across the different PSP variants and have not utilized the new MDS-PSP criteria to diagnose each variant (Whitwell et al., 2017). The lack of knowledge concerning the neuroimaging features of the atypical PSP variants limits our understanding of the pathophysiology of these variants and limits our ability to develop generalizable disease biomarkers across the PSP spectrum. This is critical since one of the goals of the MDS-PSP diagnostic criteria was to allow patients with atypical PSP to be diagnosed in a standardized manner and hence included in future clinical treatment trials for PSP. Midbrain volume has performed well as a disease biomarker in studies of PSP-RS (Paviour et al., 2007; Whitwell et al., 2012; Tsai et al., 2016), although it is unclear whether it would be an appropriate biomarker across all PSP variants or whether there are more appropriate neuroimaging targets.

The aim of this study was to assess patterns of atrophy and [^{18}F] flortaucipir uptake across these PSP variants in order to better understand differences and commonalities across variants. Specifically, we used these two neuroimaging modalities to probe the relative involvement of brainstem, subcortical and cortical systems that have been implicated pathologically in PSP to determine whether we can identify different patterns of involvement across these systems. We also report semi-quantitative tau burden results for a subset of patients that underwent autopsy.

2. Methods

2.1. Patient recruitment

One hundred and five patients with PSP were recruited by the Neurodegenerative Research Group (NRG) from the Department of Neurology, Mayo Clinic, between September 2009 and September 2018. All patients underwent a neurological evaluation that included testing on the PSP Rating Scale (Golbe and Ohman-Strickland, 2007) to assess disease severity, the Movement Disorders Society sponsored revision of the Unified Parkinson's Disease Rating Scale part III (Goetz et al., 2007) to assess motor parkinsonism, the PSP Oculomotor Impairment Scale (Whitwell et al., 2011) to assess eye movement abnormalities, the Frontal Assessment Battery (Dubois et al., 2000) to assess executive dysfunction and the Montreal Cognitive assessment Battery (Nasreddine et al., 2005) to assess general cognitive impairment. All patients seen from 2012 onwards (including all 23 PSP-SL patients) were also seen by a Speech-Language Pathologist who determined the presence/absence of apraxia of speech and agrammatic aphasia, as previously described (Josephs et al., 2012). The severity of apraxia of speech was rated using the Apraxia of Speech Rating Scale (Strand et al., 2014).

All patients were given a PSP syndromic diagnosis according to the MDS-PSP criteria (Hoglinger et al., 2017; Grimm et al., 2019). The criteria were applied based on clinical judgment and using operational definitions that we have previously published (Whitwell et al., 2019). These operational definitions use scores from the PSIS, PSP Rating Scale, and MDS-UPDRS III to determine whether a patient meets each level of the oculomotor, postural instability and akinesia sections of the MDS-PSP criteria. The criteria were retrospectively applied to cases evaluated before 2017 (n = 55) using these same operational definitions. The multiple allocations extinction (MAX) criteria were also utilized in situations when patients met criteria for more than one diagnostic label (Grimm et al., 2019). Of the 105 patients, 53 patients were clinically diagnosed with probable PSP-RS, 12 patients with probable PSP-P, five patients with probable PSP-F, four patients with PSP-PGF, 23 patients with possible PSP-SL, and eight patients with possible PSP-CBS. Of these patients, 22 have undergone autopsy and 21 have a definite autopsy confirmed diagnosis of PSP (ten PSP-RS, three PSP-CBS, three PSP-P, two PSP-SL, two PSP-F, one PSP-PGF). The remaining patient (PSP-SL) had a diagnosis of globular glial tauopathy.

All patients underwent a 3T head MRI, and a subset of 59 patients underwent [^{18}F]flortaucipir PET. Flortaucipir scans were performed a median of 1 day (inter-quartile range 1–1) from the MRI. Thirty cognitively unimpaired healthy controls were also consecutively recruited between April 2016 and September 2018 and underwent 3T head MRI and [^{18}F]flortaucipir PET imaging.

2.2. Neuroimaging analysis

All patients and controls underwent a standardized MRI protocol at 3T that included a magnetization prepared rapid gradient echo (MPRAGE) sequence (Jack et al., 2008). The majority of the cohort (78%) was scanned on a General Electric 3T scanner, although 30 patients were scanned on a Siemens Prisma 3T scanner. Tau-PET scans were acquired using a PET/CT scanner (GE Healthcare, Milwaukee, Wisconsin) operating in 3D mode. An intravenous bolus injection of 370MBq (range 333–407 MBq) of [^{18}F]flortaucipir was administered, followed by a 20-minute PET acquisition performed 80-minutes after injection. Emission data was reconstructed into a 256 × 256 matrix with a 30-cm field of view (Pixel size = 1.0 mm, slice thickness = 1.96 mm). Individual frames of the dynamic series were omitted if motion was detected, and then a mean image was created.

Voxel-level comparisons of MRI grey and white matter volumes and [^{18}F]flortaucipir uptake were performed using SPM12 (Ashburner et al., 2014). All MPRAGE scans were normalized to the Mayo Clinic Adult Lifespan Template (MCALT) using Advanced Normalization Tools (Avants et al., 2008), segmented via unified segmentation (Ashburner and Friston, 2005) with MCALT priors/settings (Schwarz et al., 2017) and grey and white matter images were modulated and smoothed at 8 mm full-width-at-half-maximum. Flortaucipir images were co-registered to the MPRAGE using 6°-of-freedom registration in SPM12. All voxels in the MPRAGE-space flortaucipir images were divided by median uptake in the cerebellar crus grey matter to create standardized uptake value ratio (SUVR) images. SUVR images were normalized to MCALT and smoothed at 6 mm full-width-at-half-maximum. Voxel-wise t-tests in SPM12 were used to compare the PSP variants to controls and against each other, including age, gender and scanner manufacturer as covariates. Results were assessed after family wise error (FWE) correction for multiple comparisons at $p < 0.05$ or uncorrected at a threshold of $p < 0.001$.

Region-level data was also outputted to assess specific structures of interest. The MCALT atlas was used to assess volume and flortaucipir uptake in subcortical grey matter structures (thalamus, globus pallidus, putamen and caudate) and cortical regions of interest. The cortical regions of interest included the supplementary motor area, superior frontal gyrus, medial prefrontal gyrus, inferior frontal gyrus (inferior frontal triangularis + inferior frontal operculum), precentral cortex, postcentral cortex and superior parietal lobe. These regions were selected as they have been previously shown to be involved in PSP-RS and in patients with apraxia of speech/agrammatic aphasia and corticobasal syndrome. The Deep Brain Stimulation Intrinsic Template (Ewert et al., 2018) atlas was used to output volume and flortaucipir uptake in the substantia nigra, subthalamic nucleus and red nucleus. These nuclei show tau deposition at autopsy in PSP and form critical components of the subcortical circuitry affected by PSP (Dickson et al., 2010). Lastly, we used in-house developed midbrain and cerebellar dentate nucleus atlases. These atlases were created by manually drawing these structures onto the MCALT template using published segmentation guidelines (Fujiwara et al., 2011). Using the parameters from normalizing the MPRAGE scans to the MCALT template, the atlases were propagated to native MPRAGE space and used to output region-level data for volume and flortaucipir SUVR. Total intracranial volume was also measured to allow the correction of head size in the MRI analyses. Region-level flortaucipir analyses were also assessed after performing a two compartment partial volume correction.

2.3. Neuropathological analyses

All autopsy cases had undergone a standard neuropathological examination performed according to the recommendations of the Consortium to Establish a Registry for Alzheimer's disease. After removal of the brain, one hemisphere was fixed in 10% buffered formaldehyde for 7–10 days followed by the taking of 7μ sections. All samples were processed in paraffin and had been stained with hematoxylin and eosin, glial fibrillary acid protein and modified Bielschowsky or Bodian silver. Immunohistochemical analysis was also performed with a battery of antibodies, including phospho-tau (CP13: gift from Dr. Peter Davis, Albert Einstein College of Medicine, Bronx, NY or clone AT8, 1:1000; Innogenetics, Alpharetta, GA). All brain tissue slides were reviewed by DWD and pathological diagnoses were rendered according to published pathological criteria for PSP. PSP was diagnosed if there were neurofibrillary tangles, coiled bodies, neuronal and glial threads, and tufted astrocytes in cardinal nuclei. Tau burden was assessed using slides immunostained with CP13 from the dentate nucleus of the cerebellum, midbrain tegmentum, substantia nigra, red nucleus, subthalamic nucleus, ventral thalamus, globus pallidus, striatum, superior frontal cortex and motor cortex for the 21 cases with definite PSP. Burden of neurofibrillary tangles (including pre-tangles), coiled bodies, tufted astrocytes, and threads in each region were recorded using a semi-quantitative 4-point scale (0 = absent, 1 = mild, 2 = moderate, 3 = severe). All semi-quantitative scoring was performed by a neuropathologist (DWD).

2.4. Statistical analysis

We used linear mixed-effects models to evaluate group-wise difference in log-transformed volume or SUVR within each region with age at scan, scanner manufacturer (General Electric vs Siemens), and total intracranial volume (for volume analysis only) as covariates. Graphical inspection of the data by manufacturer did not suggest a clear systematic manufacturer difference across regions nor were our model estimates particularly sensitive to whether or not we combined GE and Siemens scans. The mixed models included controls and modeled patient group as a random intercept, thereby shrinking group-wise estimates towards a common mean. The shrinkage, or penalized estimation, inherent in mixed model estimation reduces over-fitting and bias, and reduces false positives when performing pairwise comparisons across multiple groups (Gelman and Hill, 2007). All statistical analyses were performed using R statistical software. For all but two regional analyses, models were fit using the lmer mixed model function in the lme4 package. For the postcentral and superior parietal volumetric models the lmer estimates indicated the variance component for the random intercept was zero. Therefore, for these two regions, we used the blme package which extends lmer models so that variance components are “non degenerate” or bounded away from zero (Chung et al., 2013). We used posterior simulations using the sim function in the arm package to get confidence intervals for each group (Gelman and Hill, 2007). We report 84% and 95% CIs for the group means. Because the groups are independent, 84% CIs provide a heuristic to facilitate pairwise comparisons; 84% CIs that do not overlap indicate a significant group-wise difference at $p < 0.05$ (Knol et al., 2011). To obtain p-values for group-wise comparisons, we used the duality between confidence intervals and hypothesis tests and report the p-value for a group-wise comparison as the alpha level corresponding to the widest CI that does not include zero. For example, a 90% confidence interval for a difference between groups that does not include zero indicates $p < 0.10$; a 95% CI that does not include zero indicates $p < 0.05$, etc.

3. Results

3.1. Demographics and clinical performance

The PSP variants did not differ in gender, education, age at onset or performance on the PSP Rating Scale (Table 1). However, we did observe a difference across variants in disease duration, with the longest disease durations observed in PSP-P and PSP-SL. The age at MRI also differed, with oldest age observed in PSP-SL and PSP-PGF. Performance on tests of cognitive impairment and executive dysfunction differed across variants, with worse performance in PSP-SL, PSP-CBS and PSP-F.

Table 1
Demographics and clinical findings across PSP variants.

	PSP-RS (53)	PSP-P (12)	PSP-PGF (4)	PSP-SL (23)	PSP-CBS (8)	PSP-F (5)	Overall P-value
No. Female (%)	24 (45%)	4 (33%)	2 (50%)	15 (65%)	5 (62%)	3 (60%)	0.46
APOE ε4 carriers	6 (22%)	2 (25%)	0 (0%)	2 (10%)	1 (33%)	NA	0.55
Education	15 [13, 16]	15 [13, 18]	15 [14, 16]	15 [12, 16]	12 [10, 14]	NA	0.45
Age at scan, yrs	68 [65, 72]	70 [66, 74]	75 [73, 79]	75 [72, 80]	72 [67, 76]	69 [67, 74]	0.006
Age at onset, yrs	65 [61, 69]	63 [57, 68]	72 [69, 76]	68 [66, 72]	67 [63, 72]	65 [64, 71]	0.10
Disease duration	3.4 [2.0, 4.0]	6.6 [4.8, 8.5]	2.5 [2.0, 3.0]	6.3 [4.2, 7.6]	3.8 [3.0, 4.0]	3.4 [2.0, 4.0]	<0.001
MoCA (/30)	23 [20, 26]	24 [24, 28]	26 [26, 26]	19 [16, 25]	22 [21, 26]	19 [8, 26]	0.03
FAB (/18)	14 [12, 15]	14 [14, 16]	14 [12, 15]	11 [8, 14]	12 [9, 14]	13 [10, 16]	0.02
MDS-UPDRS III (/132)	41 [31, 51]	48 [38, 57]	45 [36, 54]	54 [34, 68]	48 [42, 56]	40 [33, 42]	0.054
PSP Rating Scale (/100)	40 [32, 49]	39 [35, 42]	40 [36, 45]	47 [36, 59]	43 [36, 53]	43 [36, 50]	0.40
PSP Rating Scale gait-midline (/20)	11 [6, 15]	13 [10, 16]	14 [13, 16]	12 [9, 14]	13 [11, 16]	12 [10, 16]	0.68
PSP oculomotor impairment scale (/5)	3 [3, 4]	2 [2, 3]	2 [2, 2]	2 [2, 3]	3 [3, 3]	2 [2, 3]	0.002
Apraxia of Speech Rating Scale II (/64)	5 [2, 7]	3 [1, 4]	2 [2, 4]	24 [16, 36]	7 [1, 11]	NA	<0.001

Data shown as N (%) or median [inter-quartile range]. P values calculated using analysis of variance regression. MDS-UPDRS = Movement Disorders Society Sponsored revision of the Unified Parkinson's Disease Rating Scale; MoCA = Montreal cognitive Assessment Battery; FAB = Frontal Assessment Battery; NA = not available.

Worse oculomotor impairment was observed in PSP-RS and PSP-CBS. These findings were similar in the subset of patients that underwent flortaucipir PET (Supplementary Table 1).

3.2. MRI volume analyses

In the voxel-level analysis (Fig. 1), grey matter volume loss was observed throughout the frontal lobes and precentral cortex of the PSP-SL variant compared to controls (FWE corrected). Frontal grey matter loss was also observed in the PSP-CBS and PSP-F variants, particularly in the prefrontal cortex, compared to controls (FWE corrected). The PSP-RS, PSP-F, PSP-CBS and PSP-SL variants showed areas of loss around the edge of the ventricles and in the hemispheric fissure, while PSP-P showed areas of loss round the edge of the ventricles (uncorrected). White matter volume loss was observed in the midbrain and superior cerebellar peduncle in PSP-RS, PSP-F and PSP-CBS (FWE corrected); midbrain only white matter volume loss was seen in PSP-P and PSP-PGF (uncorrected) compared to controls. White matter loss was observed underlying the posterior frontal and precentral cortex, and body of the corpus callosum, in PSP-SL (FWE corrected), in the posterior frontal lobes of PSP-F and PSP-CBS (uncorrected), and body of the corpus callosum in PSP-CBS (uncorrected), compared to controls.

On direct comparison between variants, PSP-SL showed greater grey and white matter loss in the premotor and motor cortex compared to PSP-RS and PSP-P (FWE corrected), with greater loss in the body of the corpus callosum when uncorrected at $p<0.001$. PSP-SL had greater premotor grey matter loss compared to PSP-CBS and greater premotor white matter loss compared to PSP-PGF and PSP-F (uncorrected). PSP-SL also showed greater grey matter loss in the thalamus compared to PSP-RS (uncorrected). PSP-CBS showed greater grey and white matter loss in the frontal lobe compared to PSP-P (uncorrected). PSP-F showed greater white matter loss in the superior cerebellar peduncle and greater grey matter loss in the frontal lobe compared to PSP-P (uncorrected).

In the ROI-level analysis, significant differences were observed across PSP variants in midbrain ($p = 0.002$), red nucleus ($p<0.001$), subthalamic nucleus ($p = 0.001$), supplementary motor area ($p = 0.002$) and precentral cortex ($p<0.001$), with trends ($p<0.10$) observed for substantia nigra and the dentate nucleus of the cerebellum (Supplementary Table 2). The inter-variant comparisons were based on the linear mixed effects model results shown in Fig. 2. PSP-RS showed smaller midbrain volumes compared to PSP-SL ($p<0.001$) and PSP-P ($p = 0.02$). PSP-CBS and PSP-F also showed smaller midbrain volumes compared to PSP-SL ($p = 0.006$ for both). Similar results were observed with the red nucleus and substantia nigra, except that PSP-F also showed smaller volumes of the red nucleus compared to PSP-P ($p = 0.02$). The PSP-SL group had larger subthalamic nucleus volumes compared to PSP-RS ($p<0.001$), PSP-F ($p = 0.001$), PSP-CBS ($p = 0.01$) and PSP-P ($p = 0.04$). The PSP-SL group showed smaller volumes of the precentral cortex compared to all other variants ($p<0.001$ vs. PSP-RS and PSP-P, $p = 0.001$ vs. PSP-CBS, $p = 0.02$ vs. PSP-PGF, $p = 0.03$ vs. PSP-P), and smaller volumes of supplementary motor area compared to all variants, except for PSP-PGF ($p<0.001$ vs. PSP-RS, $p = 0.001$ vs. PSP-F, $p = 0.01$ vs. PSP-CBS, $p = 0.04$ vs. PSP-P). No differences were observed across PSP variants in volume of dentate nucleus of the cerebellum, thalamus, pallidum, putamen, caudate, medial prefrontal, superior frontal, postcentral or superior parietal ROIs.

3.3. Flortaucipir analyses

In the voxel-based analysis (Fig. 3), PSP-RS showed elevated uptake of flortaucipir in the pallidum, putamen, thalamus, subthalamic nucleus and red nucleus (FWE corrected), with milder increased uptake in the caudate, midbrain (involving the superior aspects of the substantia nigra), dentate nucleus of the cerebellum and cerebellar grey matter (uncorrected), compared to controls. The PSP-SL variant showed elevated uptake in the pallidum, putamen, thalamus and frontal lobe with greater uptake in the left hemisphere (FWE corrected), and milder uptake in the subthalamic nucleus, midbrain (red nucleus and substantia nigra) and cerebellar grey matter compared to controls (uncorrected). More focal patterns of uptake were observed in PSP-P and PSP-PGF, with both variants showing uptake only in the putamen and pallidum compared to controls after FWE correction. At a more lenient uncorrected $p<0.001$ threshold, both variants also showed elevated uptake in the caudate and thalamus, with PSP-PGF also showing one area of increased uptake in the superior lateral premotor cortex. The PSP-CBS variant did not show any regions of elevated flortaucipir uptake compared to controls (uncorrected). The flortaucipir scans from the three PSP-CBS patients are shown in Fig. 4. Patterns of uptake were variable across the three PSP-CBS patients, with the oldest patient showing symmetric uptake in the dentate nucleus of the cerebellum, midbrain, basal ganglia, thalamus and superior posterior frontal lobe, and the other two showing milder patterns of uptake. The PSP-SL variant showed greater uptake in the frontal lobes not seen in PSP-RS, PSP-P and PSP-CBS, although only the findings compared to PSP-RS and PSP-P survived correction for multiple comparisons in the voxel-level analysis.

In the ROI-level analysis, significant differences were observed across PSP variants in precentral cortex ($p = 0.03$) and supplementary motor area ($p = 0.02$), with a trend for differences in the putamen ($p = 0.07$) (Supplementary Table 3). The inter-variant comparisons are

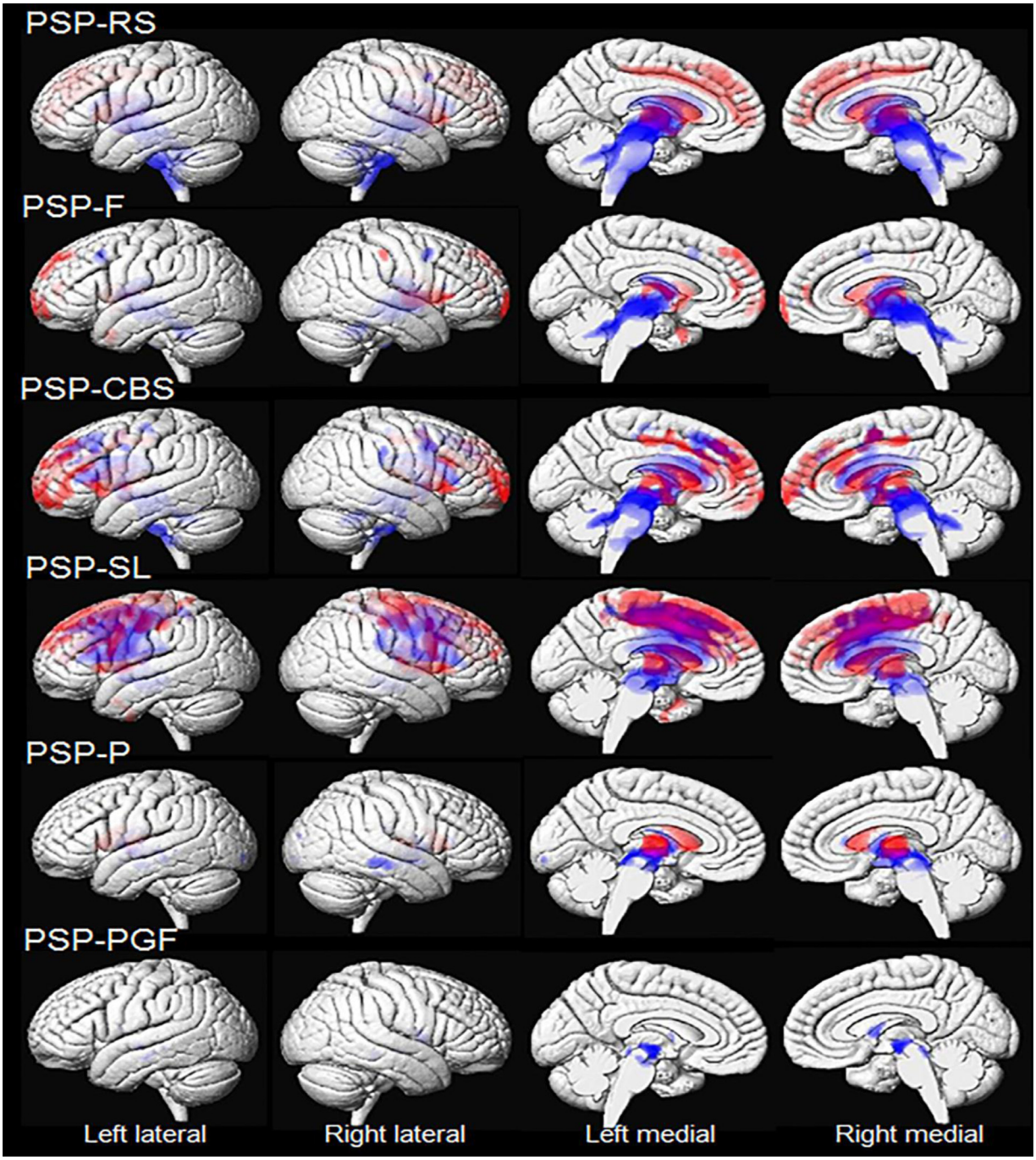

Fig. 1. Three-dimensional brain renderings showing patterns of grey (shown in red) and white (shown in blue) matter volume loss in each PSP variant compared to controls. Results are uncorrected for multiple comparisons at $p < 0.001$.(For interpretation of the references to colour in this figure legend, the reader is referred to the web version of this article.)

based on the linear mixed effects model results shown in Fig. 5. The PSP-SL group showed greater uptake in the precentral cortex and supplementary motor area compared to both PSP-RS ($p = 0.004$ and $p = 0.003$) and PSP-P ($p = 0.03$ and $p = 0.03$). The PSP-P group showed greater uptake in the putamen compared to PSP-RS ($p = 0.04$). The results were very similar with partial volume correction, except that PSP-SL also showed greater uptake in the precentral cortex and supplementary motor area compared to PSP-PGF ($p = 0.02$ and $p = 0.03$) and PSP-CBS ($p = 0.04$ for both), and PSP-SL showed greater uptake in the inferior and superior frontal lobe compared to PSP-RS ($p = 0.01$ for both).

3.4. Autopsy tau burden results

Semi-quantitative tau burden results among PSP variants are shown in Fig. 6. Tau burden in the superior frontal and motor cortices was qualitatively lower in PSP-P and PSP-PGF compared to PSP-RS, PSP-SL, PSP-CBS and PSP-F across all lesions, with the greatest burden for these regions observed in PSP-SL and PSP-CBS cases. Tau burden in the striatum and thalamus was similar for all the different PSP variants, with moderate-severe pathology consistently observed for all the four lesion types, with the exception of the PSP-PGF case that had the lowest striatal tau burden. Tau burden was moderate-severe for neurofibrillary tangles, coiled bodies and threads in the subthalamic nucleus for all PSP

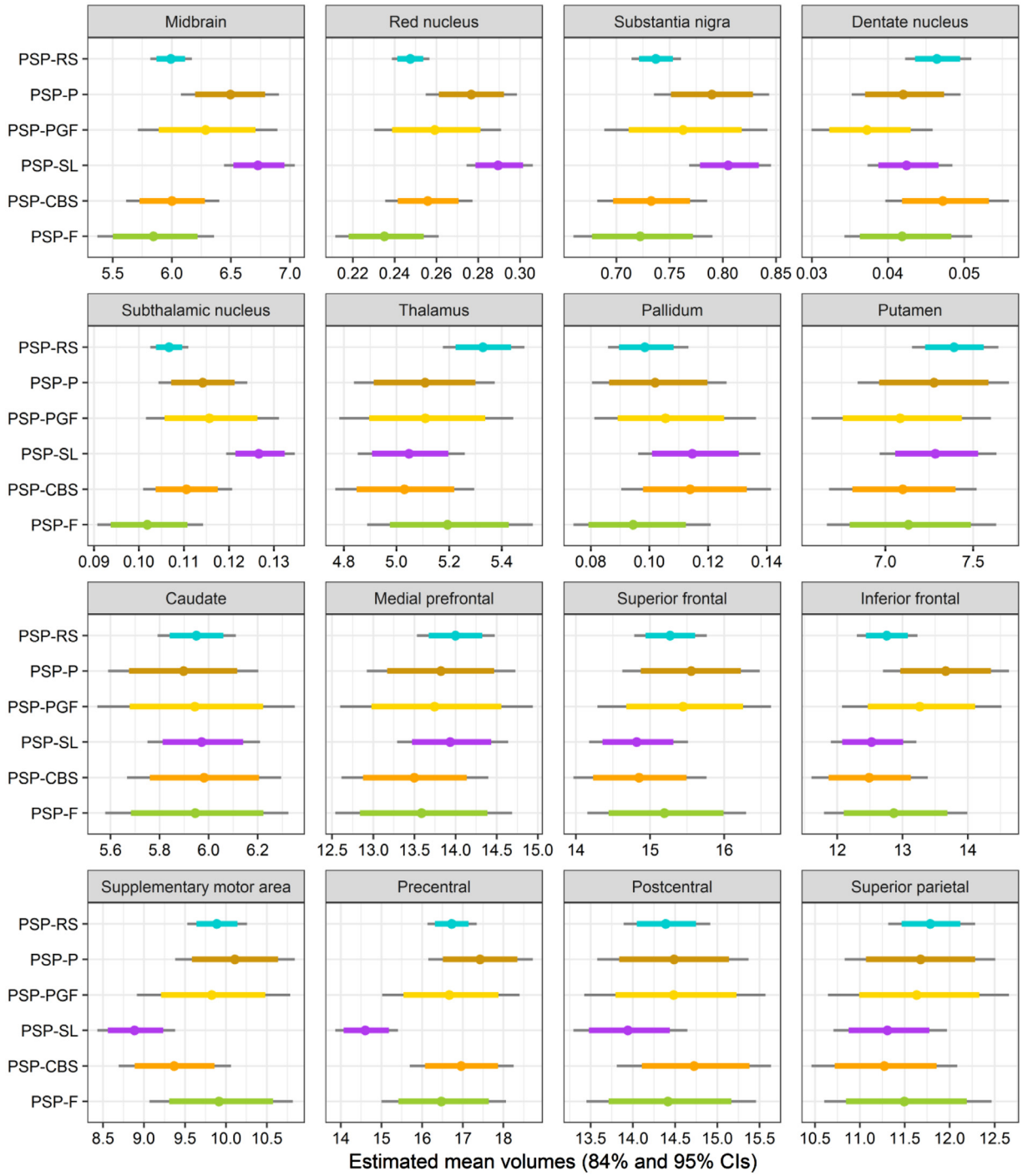

Fig. 2. Estimated log-transformed MRI volumes from Linear Mixed-Effects Models. For each boxplot the circle is the estimated mean from the model, with the thick color line showing the 84% confidence interval and the thin grey line showing the 95% confidence interval.(For interpretation of the references to colour in this figure legend, the reader is referred to the web version of this article.)

variants, except for the PSP-SL and PSP-CBS cases which showed only mild burden of coiled bodies. The PSP-SL, PSP-CBS and PSP-PGF cases showed the lowest burden of pathology in the globus pallidus. Tau burden in the substantia nigra was qualitatively higher in PSP-SL, PSP-CBS and PSP-F compared to PSP-RS, PSP-P and PSP-PGF. Tau burden in the red nucleus and midbrain tegmentum was high across all PSP variants, with PSP-RS showing the highest burden in midbrain tegmentum, and PSP-P and PSP-PGF showing the lowest burden in both regions. Burden of coiled bodies was typically low across variants in the dentate nucleus of the cerebellum, with moderate burden of neurofibrillary tangles and threads observed across variants.

4. Discussion

Our findings demonstrate that the clinical heterogeneity present in PSP is mirrored by anatomical and tau burden heterogeneity. Differences across PSP variants were observed both on MRI and flortaucipir, with the two modalities providing consistent and complementary information. While a set of subcortical structures were involved across all variants, dentatorubrothalamic tract involvement was only seen in PSP-RS, PSP-CBS and PSP-F, while cortical involvement was only characteristic of PSP-SL, PSP-CBS and PSP-F.

The neuroimaging analyses we performed allowed us to interrogate

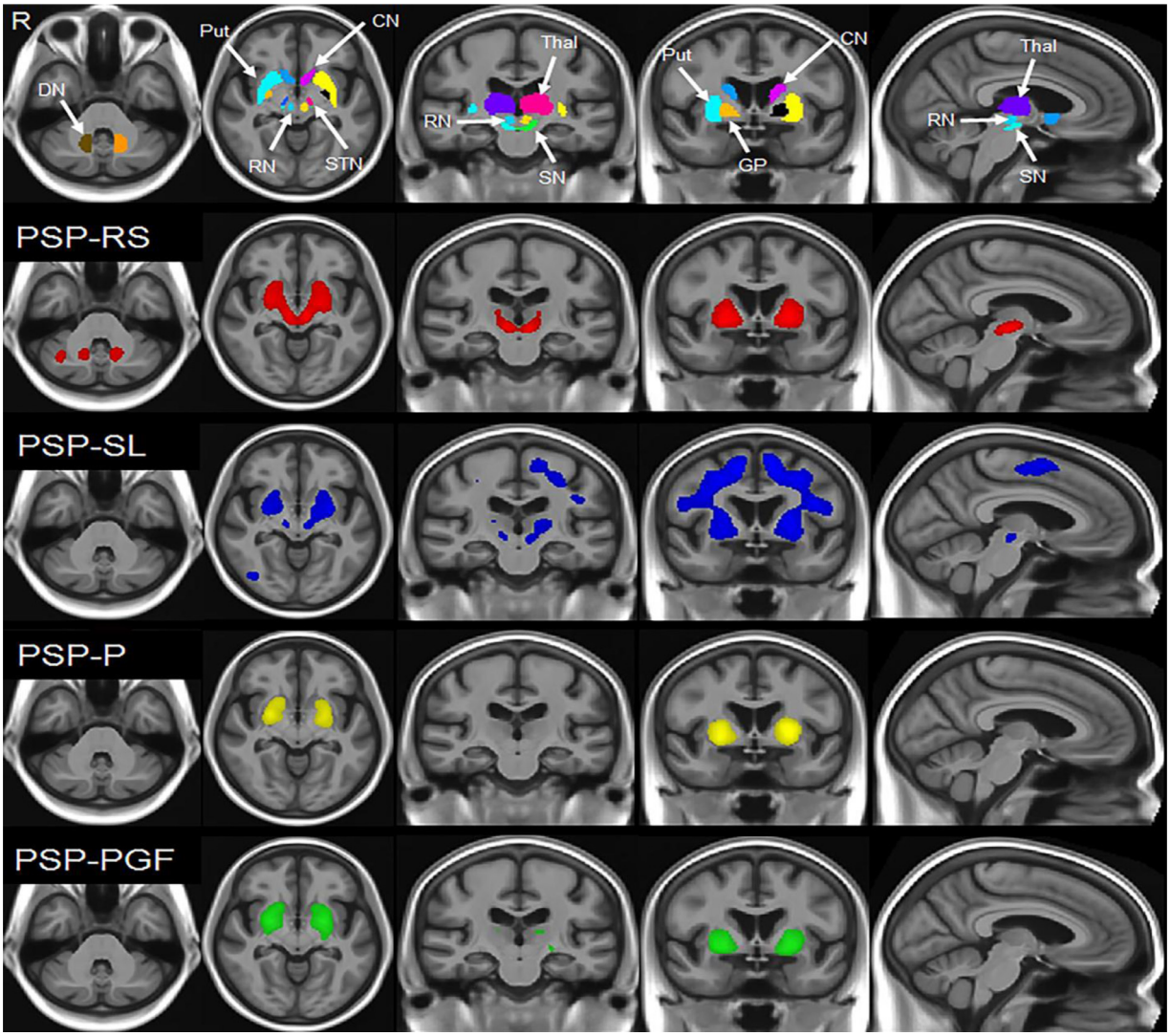

Fig. 3. Voxel-wise Flortaucipir findings in each PSP variant compared to controls. Results are shown on axial slices at the level of the dentate nucleus of the cerebellum and at the level of the red nucleus and subthalamic nucleus; coronal slices at the level of motor cortex and premotor cortex; and a sagittal slice at the level of the red nucleus. Results for the PSP-RS variant are shown in red, the PSP-SL variant in blue, the PSP-P variant in yellow and the PSP-PGF variant in green. Results are uncorrected for multiple comparisons at $p<0.001$. Top row illustrates the location of the subcortical nuclei from the atlases. DN = dentate nucleus of the cerebellum; Put = putamen; CN = caudate nucleus; RN = red nucleus; STN = subthalamic nucleus; SN = substantia nigra; Thal = thalamus; GP = globus pallidus; *R* = right.(For interpretation of the references to colour in this figure legend, the reader is referred to the web version of this article.)

the system of subcortical circuitry that is typically involved pathologically in PSP. Our findings showed that each of the PSP variants affects a different set of structures within this system (Fig. 7). The typical PSP-RS variant showed involvement of the entire subcortical system on neuroimaging. We found evidence for volume loss and flortaucipir uptake in the midbrain (including the red nucleus and substantia nigra), striatum and subthalamic nucleus, with volume loss of the superior cerebellar peduncle and flortaucipir uptake in the globus pallidus, thalamus and dentate nucleus of the cerebellum. These findings concur with previous neuroimaging findings in PSP-RS from our group and others (Josephs et al., 2008; Boxer et al., 2006; Agosta et al., 2010; Whitwell et al., 2011; Cho et al., 2017; Passamonti et al., 2017; Schonhaut et al., 2017; Whitwell et al., 2018, 2017; Smith et al., 2017) and concur with autopsy findings in PSP-RS (Dickson et al., 2010). We did not find evidence of involvement of the frontal lobe or body of the corpus callosum in our PSP-RS cohort, although mild atrophy and flortaucipir uptake have been observed in these regions in other PSP-RS cohorts (Josephs et al., 2008; Brenneis et al., 2004; Whitwell et al., 2011; Schonhaut et al., 2017; Whitwell et al., 2017; Rosskopf et al., 2014). Differences across studies may be due to the use of different statistical thresholds and different methodology, with previous studies utilizing diffusion tensor imaging for example (Whitwell et al., 2011; Rosskopf et al., 2014). Our PSP-RS findings demonstrate disruption of the dentatorubrothalamic tract which projects from the dentate nucleus of the cerebellum, through the superior cerebellar peduncle to the red nucleus and then on to the ventrolateral thalamus and motor cortex, as well as disruption of the nigrostriatal pathway, striatopallidal projections, projections between the globus pallidus and subthalamic nucleus, and projections from globus pallidus to ventrolateral thalamus that in turn project to the premotor cortex. Disruptions in the dopaminergic nigrostriatal pathway in PSP-RS have been demonstrated at post mortem (Ruberg et al., 1985) and with dopaminergic imaging studies (Brooks et al., 1990). One would hypothesize that projections from the cortex to subcortical structures may be less disrupted in PSP-RS.

Similar patterns of involvement of subcortical circuitry were observed in PSP-CBS and PSP-F, revealing substantial overlap with PSP-RS (Fig. 7). Both PSP-CBS and PSP-F showed evidence for atrophy of the superior cerebellar peduncle, midbrain, striatum, globus pallidus, subthalamic nucleus and thalamus. The main difference from PSP-RS is that both PSP-CBS and PSP-F showed evidence for volume loss in the

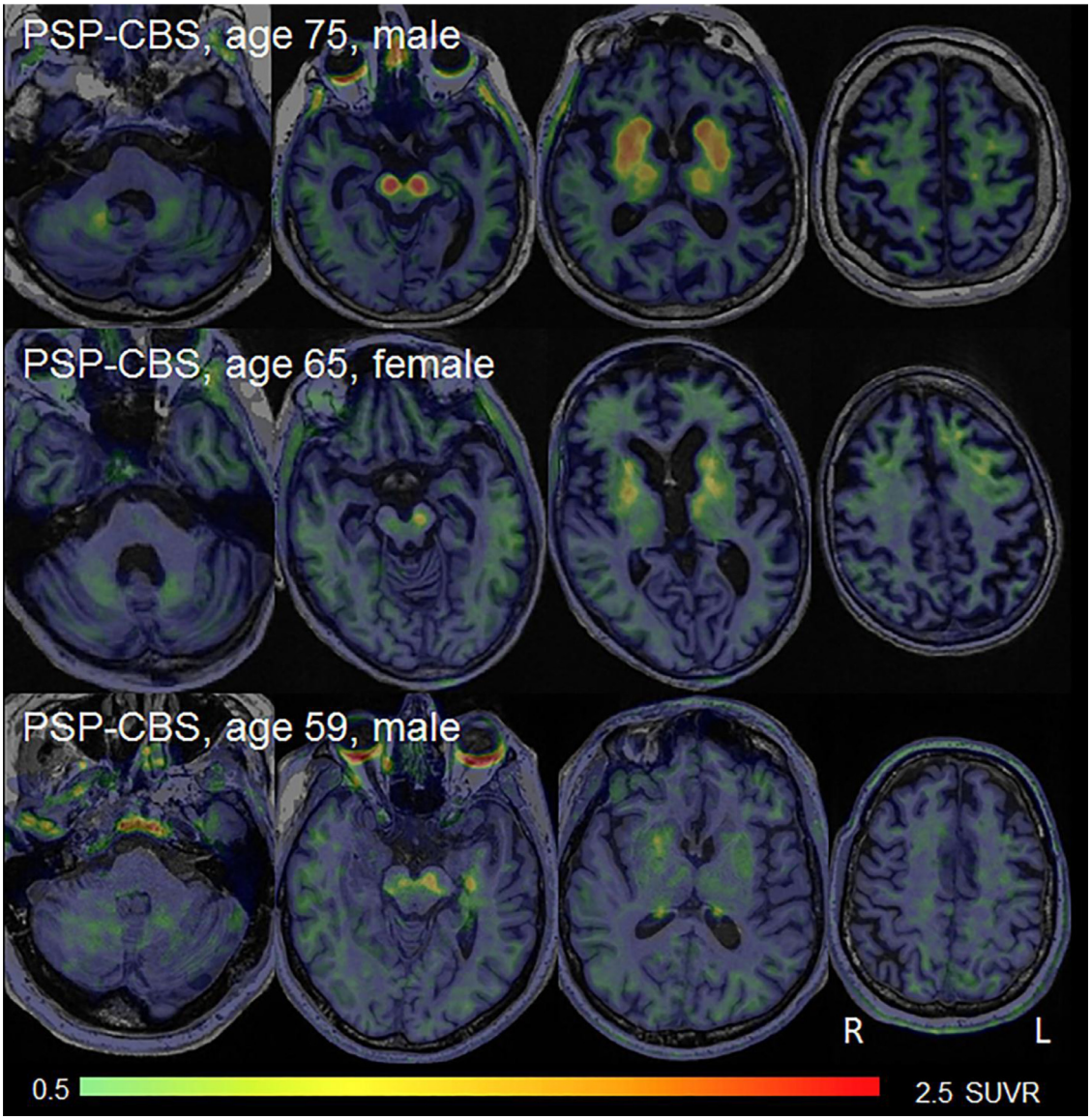

Fig. 4. Flortaucipir SUVR images for the three PSP-CBS patients.

frontal lobes, reflecting the development of cortical-driven clinical features. The PSP-F variant showed mild atrophy of the prefrontal cortex; a region that has been associated with behavioral change and executive dysfunction (Kumfor et al., 2018; Huey et al., 2015). The PSP-CBS variant also showed involvement of the prefrontal cortex but had a greater degree of frontal white matter abnormalities including the body of the corpus callosum, frontal involvement was asymmetric, and dysfunction spread more posteriorly in the frontal lobe than in PSP-F. Involvement of the prefrontal cortex in PSP-CBS is somewhat surprising, since corticobasal syndrome typically targets more posterior regions in the frontal lobe (Whitwell et al., 2010), although the findings are consistent with previous reports of patients with features of corticobasal syndrome and PSP (Josephs et al., 2012; Lee et al., 2011). These findings may suggest predominant disruption of prefrontal circuits, which include projections to the striatum which in turn project to the globus pallidus, substantia nigra, subthalamic nucleus and onto the mediodorsal thalamus and back to the prefrontal cortex (Bonelli and Cummings, 2007). Disruption of this circuit has been associated with executive dysfunction (Bonelli and Cummings, 2007). Pathological studies have shown a cortical predominance of pathology in both PSP-F and PSP-CBS (Tsuboi et al., 2005; Bigio et al., 2001). Similarly, in our autopsy series, PSP-CBS and PSP-F showed moderate to severe levels of tau pathology in cortical regions, although they also showed high tau burden in the subcortical and brainstem nuclei.

Unfortunately, we were unable to gain much insight into the tau disease process with flortaucipir in the PSP-CBS and PSP-F variants, since we did not have any PSP-F cases with flortaucipir imaging and only three PSP-CBS patients underwent flortaucipir imaging. As a group, this small PSP-CBS cohort showed no regions of significant uptake compared to controls in the voxel-level maps, and a large amount of variability in the ROI-level findings, likely due to the small number of cases. When assessed individually, there was evidence for uptake in the basal ganglia, thalamus, midbrain, and dentate nucleus of the cerebellum in one patient, but not the others, with cortical uptake observed in two cases, of which one was asymmetric. Flortaucipir uptake in patients with corticobasal syndrome can also be varied and minimal in many cases (Ali et al., 2018). One previous PSP-CBS patient reported with flortaucipir imaging showed elevated uptake in dentate nucleus of the cerebellum, midbrain, subthalamic nucleus, globus pallidus and putamen (Schonhaut et al., 2017), fitting with the subcortical circuitry we found to be abnormal on MRI.

The PSP-SL variant showed striking atrophy and flortaucipir uptake

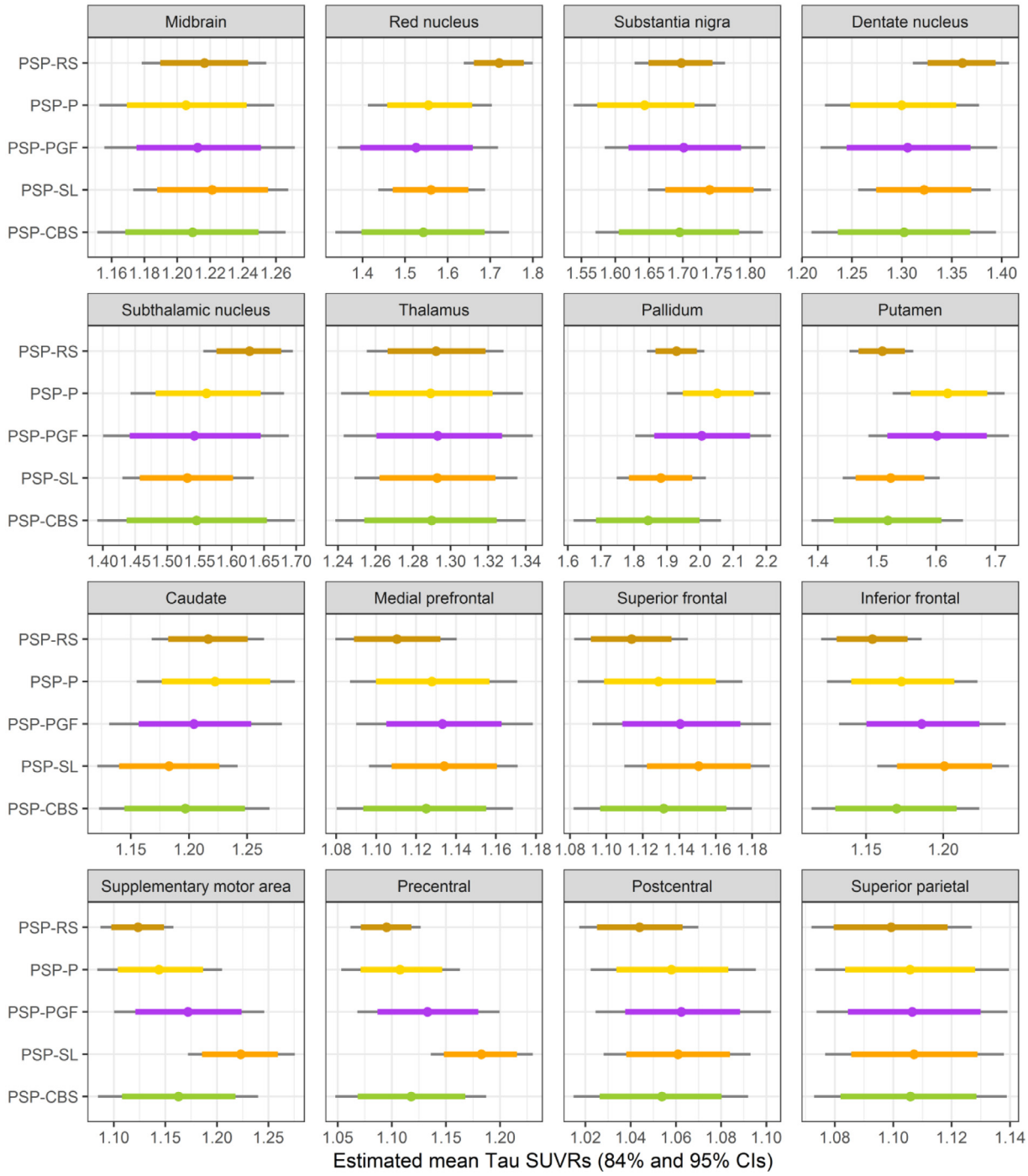

Fig.. 5. Estimated log-transformed flortaucipir SUVR from Linear Mixed-Effects Models. For each boxplot the circle is the estimated mean from the model, with the thick color line showing the 84% confidence interval and the thin grey line showing the 95% confidence interval.(For interpretation of the references to colour in this figure legend, the reader is referred to the web version of this article.)

in premotor and precentral (motor) cortex, with the degree of involvement of the supplementary motor area and precentral cortex differentiating PSP-SL from all the other PSP variants, except for PSP-CBS. This pattern of premotor and motor atrophy and flortaucipir uptake is typical for patients with a progressive apraxia of speech (Josephs et al., 2012; Utianski et al., 2018, 2018; Josephs et al., 2013; Whitwell et al., 2013). However, in contrast to PSP-RS, PSP-F and PSP-CBS, the PSP-SL variant tended to show less involvement of the infratentorial structures, including midbrain, superior cerebellar peduncle and dentate nucleus of the cerebellum (Fig. 7). This concurs with the fact that patients with progressive apraxia of speech can have isolated speech/language symptoms for many years before developing the clinical symptoms of PSP (Josephs et al., 2005; Whitwell et al., 2019; Josephs et al., 2014; Utianski et al., 2018). We have previously observed mild midbrain atrophy in patients with these speech/language impairments that develop PSP features (Whitwell et al., 2019, 2013; Josephs et al., 2014), although to a lesser degree than PSP-RS (Whitwell et al., 2013). Midbrain atrophy on MRI has also been observed in autopsy confirmed PSP-SL (Santos-Santos et al., 2016). It, therefore, appears as though infratentorial structures can become involved in PSP-SL, but are typically involved to a lesser degree than other PSP variants. Given the lack of involvement of the dentatorubrothalamic tract on neuroimaging, the

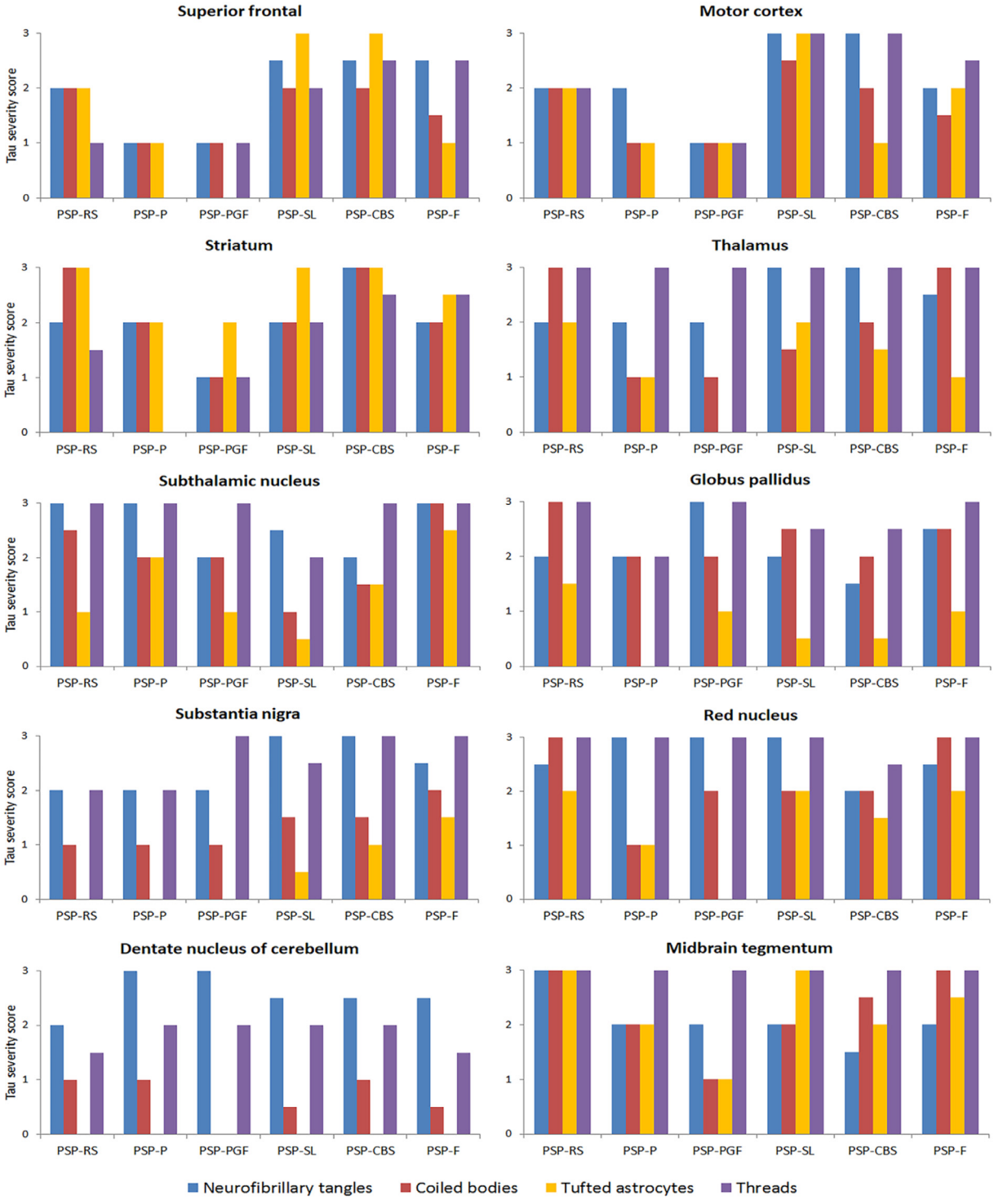

Fig. 6. Semi-quantitative tau burden measures in the autopsy confirmed PSP cases.

results may also support predominant involvement of descending cortical pathways in PSP-SL, where cortical tau burden and atrophy results in degeneration of descending corticostriatal and corticorubral pathways. The autopsy findings also showed relatively greater tau burden in the cortex and relatively lower tau burden in subthalamic nucleus and globus pallidus in PSP-SL, although tau deposition was observed in the dentate nucleus of the cerebellum and red nucleus showing some involvement of the ascending dentatorubrothalamic tract and showing that this tract can become involved before death. A previous pathological study has shown that the burden of tau pathology shifts from the subcortical and brainstem regions to the cortex in PSP-SL cases (Josephs et al., 2005).

The PSP-P and PSP-PGF variants showed much more restricted involvement of subcortical circuits compared to PSP-RS (Fig. 7). Both of these variants showed evidence for volume loss and elevated flortaucipir uptake in the striatum, globus pallidus and thalamus, and, in fact, PSP-P and PSP-PGF showed the highest flortaucipir uptake in the putamen and globus pallidus of all the PSP variants after correcting for age. This suggests that projections between the striatum, globus pallidus and subthalamic nucleus are particularly affected in PSP-P and

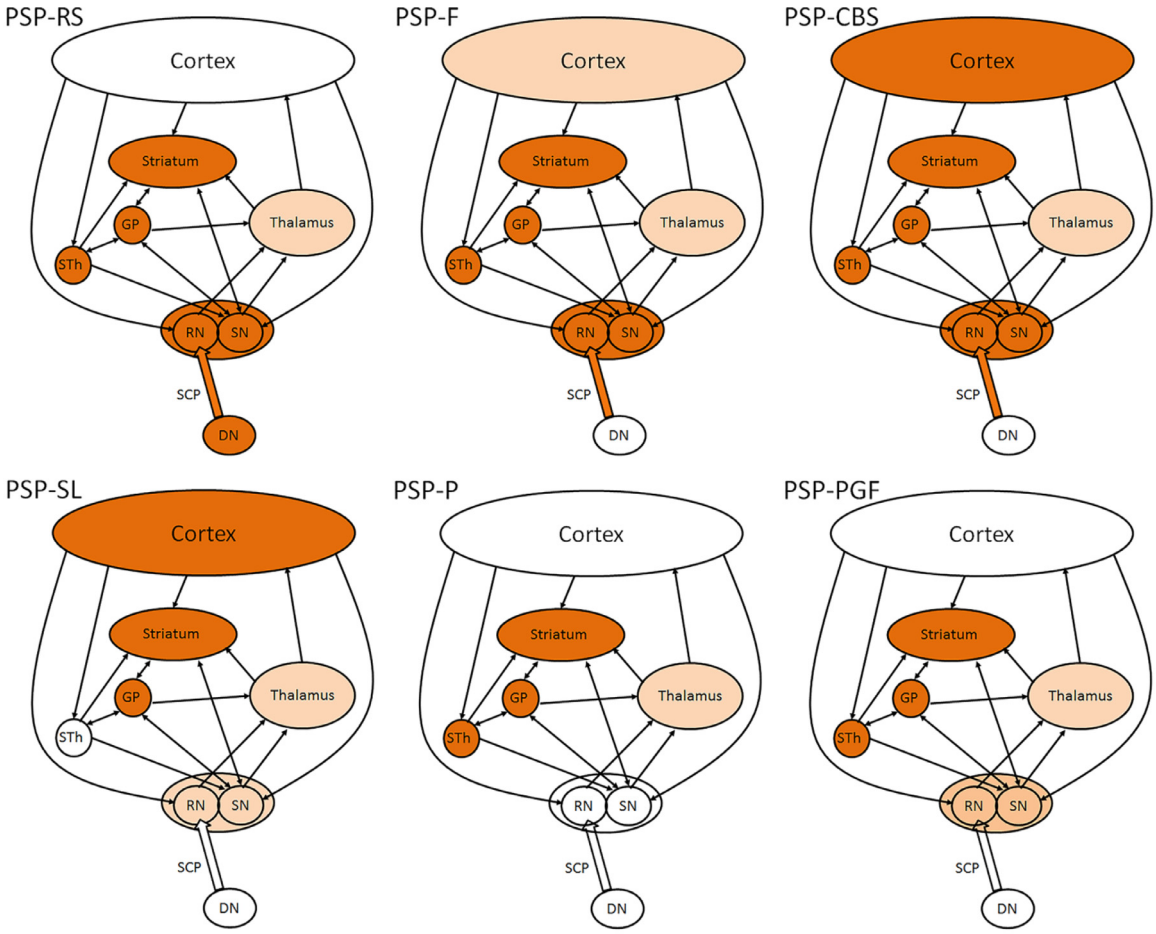

Fig. 7. Schematic depiction of the involvement of PSP-related subcortical circuitry in each PSP variant. Dark shading indicates clear involvement of a structure on neuroimaging, whereas light shading indicates mild involvement. GP =globus pallidus; STh = subthalamic nucleus; RN = red nucleus; SN = substantia nigra; DN = dentate nucleus of the cerebellum; SCP = superior cerebellar peduncle.(For interpretation of the references to colour in this figure legend, the reader is referred to the web version of this article.)

PSP-PGF. The PSP-PGF group showed mild evidence of volume loss in the midbrain, whereas PSP-P showed relatively spared midbrain volumes compared to the other PSP variants. Neither variant showed any flortaucipir uptake in the dentate nucleus of the cerebellum or volume loss of the superior cerebellar peduncle, showing a lack of evidence for involvement of the dentatorubrothalamic tract. This would support a different pattern of disease spread in these variants compared to PSP-RS with initial focus in subcortical grey matter structures. These findings concur somewhat with previous MRI studies that have shown that PSP-P patients have less atrophy of the midbrain, superior cerebellar peduncle and dentate nucleus of the cerebellum compared to PSP-RS patients (Agosta et al., 2010; Longoni et al., 2011; Agosta et al., 2012), although midbrain atrophy has been observed in PSP-P (Agosta et al., 2010; Longoni et al., 2011; Quattrone et al., 2018). There is a lack of neuroimaging studies in PSP-PGF, although volume loss of subcortical grey matter structures has been observed to a similar degree as PSP-RS (Hong et al., 2015), and case series have noted the absence of atrophy in many PSP-PGF cases (Owens et al., 2016). Flortaucipir imaging has been reported in three PSP-PGF patients and, similar to our study; elevated uptake was observed in the basal ganglia but not the dentate nucleus of the cerebellum (Schonhaut et al., 2017). Pathological studies largely confirm our neuroimaging results, finding a more restricted distribution of tau pathology in PSP-P compared to PSP-RS involving the subthalamo-nigral-pallidal system (Jellinger, 2008), with PSP-P showing similar striatal tau burden but lower tau burden in the frontal lobe and cortex compared to PSP-RS (Schofield et al., 2011). Cases of PSP-PGF have also been shown to have the greatest burden of pathology in subthalamic nucleus, globus pallidus and substantia nigra (Compta et al., 2007; Elkouzi et al., 2017), with a relative sparing of the dentate nucleus of the cerebellum compared to PSP-RS (Williams et al., 2007). Tau burden across the substantia nigra, caudate and dentate has been shown to be higher in PSP-RS compared to both PSP-PGF and PSP-P (Williams et al., 2007). Our autopsy results from PSP-P and PSP-PGF were similar, with lower burden of tau pathology in the frontal and motor cortices compared to all of the other PSP variants. There was also a tendency for PSP-P and PSP-PGF to have relatively low tau burden in the striatum, thalamus and midbrain tegmentum, particularly for coiled bodies and tufted astrocytes. Tau burden in the subthalamic nucleus and globus pallidus was similar to the other variants. We did observe moderate to severe tau deposition in neurofibrillary tangles and threads in the dentate nucleus of the cerebellum which suggests that the dentatorubrothalamic tract can become involved by the time of death even if we cannot detect abnormalities in these structures on neuroimaging.

Our findings highlight that different approaches may be needed across clinical variants in terms of neuroimaging biomarkers for clinical trials and the findings could also have diagnostic utility. The PSP-SL variant was relatively well distinguished from the other variants based on volume and flortaucipir measures from the supplementary motor area and motor cortex, and they also had a relative sparing of infratentorial regions. A relative lack of midbrain involvement in the context of motor cortex involvement may, therefore, be useful to differentiate PSP-SL from the other PSP variants. Flortaucipir uptake in the putamen was higher in PSP-P compared to PSP-RS, yet PSP-P showed smaller volumes of the midbrain and red nucleus, a signature which could be

useful in the diagnosis of PSP-P. The presence of frontal atrophy would also be suggestive of PSP-F or PSP-CBS, and the lack of atrophy of both the superior cerebellar peduncle and cortex may be suggestive of PSP-P and PSP-PGF. These neuroimaging signatures could potentially be useful in cases with an unclear clinical picture or even in the early identification of these variants. However, we did not find any measures that were helpful in differentiating PSP-CBS from PSP-F, or in differentiating PSP-P from PSP-PGF. Further work with larger numbers of patients will be needed to clarify patterns in some of these variants, determine generalizability of the results and to develop optimum diagnostic biomarkers. A number of structures within the subcortical circuits, including the striatum, thalamus, and globus pallidus, were involved across all PSP variants. This may tell us something about shared pathophysiological mechanisms across the variants, and how these structures and their projections may be particularly important for the development of shared clinical features, such as parkinsonism, postural instability and oculomotor impairment. It is possible that imaging measures from these subcortical structures may also prove to be fruitful disease biomarkers that could be applied across PSP variants, or even potential biomarkers of PSP pathology (Whitwell et al., 2017), although further studies assessing the relationship between imaging measures and disease progression, and autopsy confirmation will be needed to support these hypotheses.

The strengths of this study are the fact that we used two fundamentally different imaging modalities to probe the involvement of the key PSP-related regions across a number of PSP variants. While we had large numbers of PSP-RS, PSP-P and PSP-SL patients, the numbers of PSP-PGF and PSP-F patients were small, which was a limitation. In addition, we did not have any patients representing the PSP-oculomotor and PSP-postural instability variants. The fact that our MRI scans were performed on two different scanners could also have added variability into the analysis, although we included scanner type in our statistical analyses. Disease duration differed across the PSP variants, with longest disease duration observed in PSP-P and PSP-SL. This is typical of these two variants since both are characterized by the presence of non-PSP clinical features early in the disease course. Another limitation is that we did not have autopsy confirmation for all cases. We did not perform correlation analyses between MRI volumes and tau burden in this study due to the relative small number of autopsy cases and because the time between last available scan and autopsy varied between 0.5 and 6 years. Furthermore, not many of the autopsy cases had undergone flortaucipir PET. The flortaucipir PET ligand has shown promising utility in patients with PSP and the findings in this study matched well with our MRI analysis. However, there is uncertainty concerning whether uptake truly and adequately reflects tau deposition in the brain since autoradiographic studies have shown little binding of [^{18}F]flortaucipir to the 4R tau present in PSP (Lowe et al., 2016; Marquie et al., 2015; Sander et al., 2016). Despite this, good regional correlations have been observed between 4R tau burden and flortaucipir uptake in corticobasal degeneration (Josephs et al., 2016; McMillan et al., 2016), and we have shown that regional flortaucipir measures correlate well with MRI volumes measures, at least for subcortical structures, in PSP (Sintini et al., 2019). Nevertheless, the future role of flortaucipir in PSP is unclear given the uncertainty in how well it binds 4R tau. More work is needed to truly understand the pathological basis of the flortaucipir signal in PSP and the field urgently needs PET ligands that specifically bind to 4R tau.

The results of this study demonstrate neuroanatomical differences across the clinical variants of PSP that increase our understanding of the pathophysiology of these syndromes and will be important in the development of disease biomarkers for PSP. Given the observed differences in involvement of subcortical circuitry across PSP variants, it will be important for future studies to assess the integrity of white matter tracts within these circuits. Furthermore, longitudinal studies will be needed to assess progression and the degree to which unaffected parts of these circuits become affected over time.

Funding

This study was funded by the National Institutes of Health (grants R01-NS89757, R01-DC12519, R01-DC010367 and R01-DC14942) and the Dana Foundation.

Declaration of Competing Interest

The authors do not have any competing interests to declare.

Acknowledgements

We would like to acknowledge AVID Radiopharmaceuticals for provision of AV-1451 precursor, chemistry production advice and oversight, and FDA regulatory cross-filing permission and documentation needed for this work.

Supplementary materials

Supplementary material associated with this article can be found, in the online version, at doi:10.1016/j.nicl.2019.102152.

References

Dickson, D.W., 2008. Neuropathology of progressive supranuclear palsy. Handb. Clin. Neurol. 89, 487–491.
Steele, J.C., Richardson, J.C., Olszewski, J, 1964. Progressive supranuclear palsy. a heterogeneous degeneration involving the brain stem, basal ganglia and cerebellum with vertical gaze and pseudobulbar palsy, nuchal dystonia and dementia. Arch. Neurol. 10, 333–359 Apr.
Hoglinger, G.U., Respondek, G., Stamelou, M., et al., 2017. Clinical diagnosis of progressive supranuclear palsy: the movement disorder society criteria. Mov. Disord. 32 (6), 853–864 Jun.
Litvan, I., Agid, Y., Calne, D., et al., 1996. Clinical research criteria for the diagnosis of progressive supranuclear palsy (Steele-Richardson-Olszewski syndrome): report of the NINDS-SPSP international workshop. Neurology 47 (1), 1–9 Jul.
Williams, D.R., Holton, J.L., Strand, K., Revesz, T., Lees, A.J, 2007a. Pure akinesia with gait freezing: a third clinical phenotype of progressive supranuclear palsy. Mov. Disord. 22 (15), 2235–2241 Nov 15.
Williams, D.R., de Silva, R., Paviour, D.C., et al., 2005. Characteristics of two distinct clinical phenotypes in pathologically proven progressive supranuclear palsy: Richardson's syndrome and PSP-parkinsonism. Brain 128 (Pt 6), 1247–1258 Jun.
Josephs, K.A., Eggers, S.D., Jack Jr, C.R., Whitwell, J.L, 2012a. Neuroanatomical correlates of the progressive supranuclear palsy corticobasal syndrome hybrid. Eur. J. Neurol. 19 (11), 1440–1446 Apr 23.
Tsuboi, Y., Josephs, K.A., Boeve, B.F., et al., 2005. Increased tau burden in the cortices of progressive supranuclear palsy presenting with corticobasal syndrome. Mov. Disord. 20 (8), 982–988 Aug.
Hassan, A., Parisi, J.E., Josephs, K.A, 2012. Autopsy-proven progressive supranuclear palsy presenting as behavioral variant frontotemporal dementia. Neurocase 18 (6), 478–488.
Josephs, K.A., Boeve, B.F., Duffy, J.R., et al., 2005. Atypical progressive supranuclear palsy underlying progressive apraxia of speech and nonfluent aphasia. Neurocase 11 (4), 283–296 Aug.
Josephs, K.A., Duffy, J.R., Strand, E.A., et al., 2006a. Clinicopathological and imaging correlates of progressive aphasia and apraxia of speech. Brain 129 (Pt 6), 1385–1398 Jun.
Josephs, K.A., Whitwell, J.L., Dickson, D.W., et al., 2008. Voxel-based morphometry in autopsy proven PSP and CBD. Neurobiol. Aging 29 (2), 280–289 Feb.
Josephs, K.A., Whitwell, J.L., Boeve, B.F., et al., 2006b. Rates of cerebral atrophy in autopsy-confirmed progressive supranuclear palsy. Ann. Neurol. 59 (1), 200–203 Jan.
Josephs, K.A., Xia, R., Mandrekar, J., et al., 2013a. Modeling trajectories of regional volume loss in progressive supranuclear palsy. Mov. Disord. 28 (8), 1117–1124 Jul.
Boxer, A.L., Geschwind, M.D., Belfor, N., et al., 2006. Patterns of brain atrophy that differentiate corticobasal degeneration syndrome from progressive supranuclear palsy. Arch. Neurol. 63 (1), 81–86 Jan.
Brenneis, C., Seppi, K., Schocke, M., Benke, T., Wenning, G.K., Poewe, W, 2004. Voxel based morphometry reveals a distinct pattern of frontal atrophy in progressive supranuclear palsy. J. Neurol. Neurosurg. Psychiatry 75 (2), 246–249 Feb.
Groschel, K., Kastrup, A., Litvan, I., Schulz, J.B, 2006. Penguins and hummingbirds: midbrain atrophy in progressive supranuclear palsy. Neurology 66 (6), 949–950 Mar 28.
Oba, H., Yagishita, A., Terada, H., et al., 2005. New and reliable MRI diagnosis for progressive supranuclear palsy. Neurology 64 (12), 2050–2055 Jun 28.
Paviour, D.C., Price, S.L., Stevens, J.M., Lees, A.J., Fox, N.C, 2005. Quantitative MRI measurement of superior cerebellar peduncle in progressive supranuclear palsy. Neurology 64 (4), 675–679 Feb 22.
Agosta, F., Kostic, V.S., Galantucci, S., et al., 2010. The in vivo distribution of brain tissue

loss in Richardson's syndrome and PSP-parkinsonism: a VBM-DARTEL study. Eur. J. Neurosci. 32 (4), 640–647 Aug.
Price, S., Paviour, D., Scahill, R., et al., 2004. Voxel-based morphometry detects patterns of atrophy that help differentiate progressive supranuclear palsy and Parkinson's disease. Neuroimage 23 (2), 663–669 Oct.
Whitwell, J.L., Avula, R., Master, A., et al., 2011a. Disrupted thalamocortical connectivity in PSP: a resting state fMRI, DTI, and VBM study. Parkinsonism Relat. Disord. 17 (8), 599–605.
Whitwell, J.L., Hoglinger, G.U., Antonini, A., et al., 2017a. Radiological biomarkers for diagnosis in PSP: where are we and where do we need to be? Mov. Disord. 32 (7), 955–971 Jul.
Whitwell, J.L., Master, A.V., Avula, R., et al., 2011b. Clinical correlates of white matter tract degeneration in PSP. Arch. Neurol. 68 (6), 753–760.
Whitwell, J.L., Schwarz, C.G., Reid, R.I., Kantarci, K., Jack Jr, C.R., Josephs, K.A, 2014. Diffusion tensor imaging comparison of progressive supranuclear palsy and corticobasal syndromes. Parkinsonism Relat. Disord. 20 (5), 493–498 May.
Knake, S., Belke, M., Menzler, K., et al., 2010. In vivo demonstration of microstructural brain pathology in progressive supranuclear palsy: a DTI study using TBSS. Mov. Disord Mar 10.
Padovani, A., Borroni, B., Brambati, S.M., et al., 2006. Diffusion tensor imaging and voxel based morphometry study in early progressive supranuclear palsy. J. Neurol. Neurosurg. Psychiatry 77 (4), 457–463 Apr.
Dickson, D.W., 1999. Neuropathologic differentiation of progressive supranuclear palsy and corticobasal degeneration. J. Neurol. 246 (2), II6–I15 SepSuppl.
Dickson, D.W., Ahmed, Z., Algom, A.A., Tsuboi, Y., Josephs, K.A, 2010. Neuropathology of variants of progressive supranuclear palsy. Curr. Opin. Neurol. 23 (4), 394–400 Aug.
Chien, D.T., Bahri, S., Szardenings, A.K., et al., 2013. Early clinical PET imaging results with the novel PHF-tau radioligand [F-18]-T807. J. Alzheimers Dis. 34 (2), 457–468 Jan 1.
Xia, C.F., Arteaga, J., Chen, G., et al., 2013. [(18)F]T807, a novel tau positron emission tomography imaging agent for Alzheimer's disease. Alzheimers Dement. 9 (6), 666–676 Nov.
Cho, H., Choi, J.Y., Hwang, M.S., et al., 2017. Subcortical 18 F-AV-1451 binding patterns in progressive supranuclear palsy. Mov. Disord. 32 (1), 134–140 Nov 3.
Passamonti, L., Vazquez Rodriguez, P., Hong, Y.T., et al., 2017. 18F-AV-1451 positron emission tomography in Alzheimer's disease and progressive supranuclear palsy. Brain 140 (3), 781–791 Mar 1.
Schonhaut, D.R., McMillan, C.T., Spina, S., et al., 2017. (18) F-flortaucipir tau positron emission tomography distinguishes established progressive supranuclear palsy from controls and Parkinson disease: a multicenter study. Ann. Neurol. 82 (4), 622–634 Oct.
Whitwell, J.L., Ahlskog, J.E., Tosakulwong, N., et al., 2018. Pittsburgh Compound B and AV-1451 positron emission tomography assessment of molecular pathologies of Alzheimer's disease in progressive supranuclear palsy. Parkinsonism Relat. Disord. 48, 3–9 Mar.
Whitwell, J.L., Lowe, V.J., Tosakulwong, N., et al., 2017b. [18 F]AV-1451 tau positron emission tomography in progressive supranuclear palsy. Mov. Disord. 32 (1), 124–133 Oct 27.
Smith, R., Schain, M., Nilsson, C., et al., 2017. Increased basal ganglia binding of 18 F-AV-1451 in patients with progressive supranuclear palsy. Mov. Disord. 32 (1), 108–114 Oct 6.
Williams, D.R., Holton, J.L., Strand, C., et al., 2007b. Pathological tau burden and distribution distinguishes progressive supranuclear palsy-parkinsonism from Richardson's syndrome. Brain 130 (Pt 6), 1566–1576 Jun.
Longoni, G., Agosta, F., Kostic, V.S., et al., 2011. MRI measurements of brainstem structures in patients with Richardson's syndrome, progressive supranuclear palsy-parkinsonism, and Parkinson's disease. Mov. Disord. 26 (2), 247–255 Feb 1.
Quattrone, A., Morelli, M., Williams, D.R., et al., 2016. MR parkinsonism index predicts vertical supranuclear gaze palsy in patients with PSP-parkinsonism. Neurology 87 (12), 1266–1273 Sep 20.
Santos-Santos, M.A., Mandelli, M.L., Binney, R.J., et al., 2016. Features of patients with nonfluent/agrammatic primary progressive aphasia with underlying progressive supranuclear palsy pathology or corticobasal degeneration. JAMA Neurol. 73 (6), 733–742 Jun 1.
Josephs, K.A., Duffy, J.R., Strand, E.A., et al., 2012b. Characterizing a neurodegenerative syndrome: primary progressive apraxia of speech. Brain 135 (Pt 5), 1522–1536 May.
Whitwell, J.L., Duffy, J.R., Strand, E.A., et al., 2012a. Neuroimaging comparison of primary progressive apraxia of speech and progressive supranuclear palsy. Eur. J. Neurol. 20 (4), 629–637.
Rohrer, J.D., Paviour, D., Bronstein, A.M., O'Sullivan, S.S., Lees, A., Warren, J.D, 2010. Progressive supranuclear palsy syndrome presenting as progressive nonfluent aphasia: a neuropsychological and neuroimaging analysis. Mov. Disord. 25 (2), 179–188 Jan 30.
Whitwell, J.L., Jack Jr, C.R., Parisi, J.E., et al., 2013a. Midbrain atrophy is not a biomarker of progressive supranuclear palsy pathology. Eur. J. Neurol. 20 (10), 1417–1422 Oct.
Lee, S.E., Rabinovici, G.D., Mayo, M.C., et al., 2011. Clinicopathological correlations in corticobasal degeneration. Ann. Neurol. 70 (2), 327–340 Aug.
Whitwell, J.L., Jack Jr, C.R., Boeve, B.F., et al., 2010. Imaging correlates of pathology in corticobasal syndrome. Neurology 75 (21), 1879–1887 Nov 23.
Paviour, D.C., Price, S.L., Lees, A.J., Fox, N.C, 2007. MRI derived brain atrophy in PSP and MSA-P. Determining sample size to detect treatment effects. J. Neurol. 254 (4), 478–481 Apr.
Whitwell, J.L., Xu, J., Mandrekar, J.N., Gunter, J.L., Jack Jr, C.R., Josephs, K.A, 2012b. Rates of brain atrophy and clinical decline over 6 and 12-month intervals in PSP: determining sample size for treatment trials. Parkinsonism Relat. Disord. 18 (3), 252–256.
Tsai, R.M., Lobach, I., Bang, J., et al., 2016. Clinical correlates of longitudinal brain atrophy in progressive supranuclear palsy. Parkinsonism Relat. Disord. 28, 29–35 Jul.
Golbe, L.I., Ohman-Strickland, P.A., 2007. A clinical rating scale for progressive supranuclear palsy. Brain 130 (Pt 6), 1552–1565 Jun.
Goetz, C.G., Fahn, S., Martinez-Martin, P., et al., 2007. Movement disorder society-sponsored revision of the unified Parkinson's disease rating scale (MDS-UPDRS): process, format, and clinimetric testing plan. Mov. Disord. 22 (1), 41–47 Jan.
Dubois, B., Slachevsky, A., Litvan, I., Pillon, B, 2000. The FAB: a frontal assessment battery at bedside. Neurology 55 (11), 1621–1626 Dec 12.
Nasreddine, Z.S., Phillips, N.A., Bedirian, V., et al., 2005. The Montreal cognitive assessment, MoCA: a brief screening tool for mild cognitive impairment. J. Am. Geriatr. Soc. 53 (4), 695–699 Apr.
Strand, E.A., Duffy, J.R., Clark, H.M., Josephs, K, 2014. The apraxia of speech rating scale: a tool for diagnosis and description of apraxia of speech. J. Commun. Disord. 51, 43–50.
Grimm, M.J., Respondek, G., Stamelou, M., et al., 2019. How to apply the movement disorder society criteria for diagnosis of progressive supranuclear palsy. Mov. Disord Mar 18.
Whitwell, J.L., Stevens, C.A., Duffy, J.R., et al., 2019. An evaluation of the progressive supranuclear palsy speech/language variant. Mov. Disord. Clin. Pract. 6 (6), 452–461.
Jack Jr, C.R., Lowe, V.J., Senjem, M.L., et al., 2008. 11C PiB and structural MRI provide complementary information in imaging of Alzheimer's disease and amnestic mild cognitive impairment. Brain 131 (Pt 3), 665–680 Mar.
Ashburner, J., Barnes, G., Chen, C., et al., 2014. SPM12 Manual. Wellcome Trust Centre for Neuroimaging, London, UK.
Avants, B.B., Epstein, C.L., Grossman, M., Gee, J.C, 2008. Symmetric diffeomorphic image registration with cross-correlation: evaluating automated labeling of elderly and neurodegenerative brain. Med. Image Anal. 12 (1), 26–41 Feb.
Ashburner, J., Friston, K.J, 2005. Unified segmentation. Neuroimage 26 (3), 839–851 Jul 1.
Schwarz, C.G., Gunter, J.L., Ward, C.P., et al., 2017. The Mayo clinic adult lifespan template: better quantification across the lifespan. Alzheimers Dement. 13, 792.
Ewert, S., Plettig, P., Li, N., et al., 2018. Toward defining deep brain stimulation targets in MNI space: a subcortical atlas based on multimodal MRI, histology and structural connectivity. Neuroimage 170, 271–282 Apr 15.
Fujiwara, A., Yoshida, T., Otsuka, T., et al., 2011. Midbrain volume increase in patients with panic disorder. Psychiatry Clin. Neurosci. 65 (4), 365–373 Jun.
Gelman, A., Hill, J., 2007. Data Analysis Using Regression and Multilevel/Hierarchical Models. Cambridge University Press, Cambridge; New York.
Chung, Y., Rabe-Hesketh, S., Dorie, V., Gelman, A., Liu, J, 2013. A nondegenerate penalized likelihood estimator for variance parameters in multilevel models. Psychometrika 78 (4), 685–709 2013/10//.
Knol, M.J., Pestman, W.R., Grobbee, D.E, 2011. The (mis)use of overlap of confidence intervals to assess effect modification. Eur. J. Epidemiol. 26 (4), 253–254 2011/04//.
Rosskopf, J., Muller, H.P., Huppertz, H.J., Ludolph, A.C., Pinkhardt, E.H., Kassubek, J, 2014. Frontal corpus callosum alterations in progressive supranuclear palsy but not in Parkinson's disease. Neurodegener. Dis. 14 (4), 184–193.
Ruberg, M., Javoy-Agid, F., Hirsch, E., et al., 1985. Dopaminergic and cholinergic lesions in progressive supranuclear palsy. Ann. Neurol. 18 (5), 523–529 Nov.
Brooks, D.J., Ibanez, V., Sawle, G.V., et al., 1990. Differing patterns of striatal 18F-dopa uptake in Parkinson's disease, multiple system atrophy, and progressive supranuclear palsy. Ann. Neurol. 28 (4), 547–555 Oct.
Kumfor, F., Zhen, A., Hodges, J.R., Piguet, O., Irish, M, 2018. Apathy in Alzheimer's disease and frontotemporal dementia: distinct clinical profiles and neural correlates. Cortex 103, 350–359 Jun.
Huey, E.D., Lee, S., Brickman, A.M., et al., 2015. Neuropsychiatric effects of neurodegeneration of the medial versus lateral ventral prefrontal cortex in humans. Cortex 73, 1–9 Dec.
Bonelli, R.M., Cummings, J.L., 2007. Frontal-subcortical circuitry and behavior. Dialog. Clin. Neurosci. 9 (2), 141–151.
Bigio, E.H., Vono, M.B., Satumtira, S., et al., 2001. Cortical synapse loss in progressive supranuclear palsy. J. Neuropathol. Exp. Neurol. 60 (5), 403–410 May.
Ali, F., Whitwell, J.L., Martin, P.R., et al., 2018. [(18)F] AV-1451 uptake in corticobasal syndrome: the influence of beta-amyloid and clinical presentation. J. Neurol. 265 (5), 1079–1088 May.
Utianski, R.L., Whitwell, J.L., Schwarz, C.G., et al., 2018a. Tau uptake in agrammatic primary progressive aphasia with and without apraxia of speech. Eur. J. Neurol. 25 (11), 1352–1357 Nov.
Utianski, R.L., Whitwell, J.L., Schwarz, C.G., et al., 2018b. Tau-PET imaging with [18F]AV-1451 in primary progressive apraxia of speech. Cortex 99, 358–374 Feb.
Josephs, K.A., Duffy, J.R., Strand, E.A., et al., 2013b. Syndromes dominated by apraxia of speech show distinct characteristics from agrammatic PPA. Neurology 81 (4), 337–345 Jul 23.
Whitwell, J.L., Duffy, J.R., Strand, E.A., et al., 2013b. Neuroimaging comparison of primary progressive apraxia of speech and progressive supranuclear palsy. Eur. J. Neurol. 20 (4), 629–637 Apr.
Josephs, K.A., Duffy, J.R., Strand, E.A., et al., 2014. The evolution of primary progressive apraxia of speech. Brain 137 (Pt 10), 2783–2795 Oct.
Utianski, R.L., Duffy, J.R., Clark, H.M., et al., 2018c. Clinical progression in four cases of primary progressive apraxia of speech. Am. J. Speech Lang. Pathol. 27 (4), 1303–1318 Nov 21.
Agosta, F., Pievani, M., Svetel, M., et al., 2012. Diffusion tensor MRI contributes to differentiate Richardson's syndrome from PSP-parkinsonism. Neurobiol. Aging 33 (12),

2817–2826 Dec.
Quattrone, A., Morelli, M., Nigro, S., et al., 2018. A new MR imaging index for differentiation of progressive supranuclear palsy-parkinsonism from Parkinson's disease. Parkinsonism Relat. Disord. 54, 3–8 Sep.
Hong, J.Y., Yun, H.J., Sunwoo, M.K., et al., 2015. Comparison of regional brain atrophy and cognitive impairment between pure akinesia with gait freezing and Richardson's syndrome. Front. Aging Neurosci. 7, 180.
Owens, E., Josephs, K.A., Savica, R., et al., 2016. The clinical spectrum and natural history of pure akinesia with gait freezing. J. Neurol. 263 (12), 2419–2423 Dec.
Jellinger, K.A., 2008. Different tau pathology pattern in two clinical phenotypes of progressive supranuclear palsy. Neurodegener. Dis. 5 (6), 339–346.
Schofield, E.C., Hodges, J.R., Macdonald, V., Cordato, N.J., Kril, J.J., Halliday, G.M, 2011. Cortical atrophy differentiates Richardson's syndrome from the parkinsonian form of progressive supranuclear palsy. Mov. Disord. 26 (2), 256–263 Feb 1.
Compta, Y., Valldeoriola, F., Tolosa, E., Rey, M.J., Marti, M.J., Valls-Sole, J, 2007. Long lasting pure freezing of gait preceding progressive supranuclear palsy: a clinicopathological study. Mov. Disord. 22 (13), 1954–1958 Oct 15.
Elkouzi, A., Bit-Ivan, E.N., Elble, R.J, 2017. Pure akinesia with gait freezing: a clinicopathologic study. J. Clin. Mov. Disord. 4, 15.
Lowe, V.J., Curran, G., Fang, P., et al., 2016. An autoradiographic evaluation of AV-1451 Tau PET in dementia. Acta Neuropathol. Commun. 4 (1), 58.
Marquie, M., Normandin, M.D., Vanderburg, C.R., et al., 2015. Validating novel tau positron emission tomography tracer [F-18]-AV-1451 (T807) on postmortem brain tissue. Ann. Neurol. 78 (5), 787–800 Nov.
Sander, K., Lashley, T., Gami, P., et al., 2016. Characterization of tau positron emission tomography tracer [F]AV-1451 binding to postmortem tissue in Alzheimer's disease, primary tauopathies, and other dementias. Alzheimers Dement Feb 15.
Josephs, K.A., Whitwell, J.L., Tacik, P., et al., 2016. [18F]AV-1451 tau-PET uptake does correlate with quantitatively measured 4R-tau burden in autopsy-confirmed corticobasal degeneration. Acta Neuropathol. 132 (6), 931–933 Dec.
McMillan, C.T., Irwin, D.J., Nasrallah, I., et al., 2016. Multimodal evaluation demonstrates in vivo 18F-AV-1451 uptake in autopsy-confirmed corticobasal degeneration. Acta Neuropathol. 132 (6), 935–937 Dec.
Sintini, I., Schwarz, C.G., Senjem, M.L., et al., 2019. Multimodal neuroimaging relationships in progressive supranuclear palsy. Parkinsonism Relat. Disord Jul 2.